AD_____

Award Number: W81XWH-04-1-0551

TITLE: Investigation of Metastatic Breast Tumor Heterogeneity and Progression Using Dual Optical/SPECT Imaging

PRINCIPAL INVESTIGATOR: Peter P. Antich, Ph.D., D.Sc.
Anca Constantinescu, Ph.D.
Matthew Lewis, Ph.D.
Ralph Mason, Ph.D.
Edmond Richer, Ph.D.

CONTRACTING ORGANIZATION: University of Texas Southwestern Medical Center at Dallas
Dallas, TX 75390-9105

REPORT DATE: May 2005

TYPE OF REPORT: Annual

PREPARED FOR: U.S. Army Medical Research and Materiel Command
Fort Detrick, Maryland 21702-5012

REPORT DOCUMENTATION PAGE

Form Approved
OMB No. 0704-0188

1. REPORT DATE *(DD-MM-YYYY)*	2. REPORT TYPE	3. DATES COVERED *(From - To)*
01-05-2005	Annual	1 May 04 – 30 Apr 05

4. TITLE AND SUBTITLE
Investigation of Metastatic Breast Tumor Heterogeneity and Progression Using Dual Optical/SPECT Imaging

5a. CONTRACT NUMBER

5b. GRANT NUMBER
W81XWH-04-1-0551

5c. PROGRAM ELEMENT NUMBER

6. AUTHOR(S)
Peter P. Antich, Ph.D., D.Sc., Anca Constantinescu, Ph.D., Matthew Lewis, Ph.D., Ralph Mason, Ph.D., Edmond Richer, Ph.D.

E-Mail: Peter.Antich@utsouthwestern.edu

5d. PROJECT NUMBER

5e. TASK NUMBER

5f. WORK UNIT NUMBER

7. PERFORMING ORGANIZATION NAME(S) AND ADDRESS(ES)
University of Texas Southwestern Medical Center at Dallas
Dallas, TX 75390-9105

8. PERFORMING ORGANIZATION REPORT NUMBER

9. SPONSORING / MONITORING AGENCY NAME(S) AND ADDRESS(ES)
U.S. Army Medical Research and Materiel Command
Fort Detrick, Maryland 21702-5012

10. SPONSOR/MONITOR'S ACRONYM(S)

11. SPONSOR/MONITOR'S REPORT NUMBER(S)

12. DISTRIBUTION / AVAILABILITY STATEMENT
Approved for Public Release; Distribution Unlimited

13. SUPPLEMENTARY NOTES
Original contains color plates: All DTIC reproductions will be in black and white.

14. ABSTRACT:

The goal of our project is to image tumor growth, metastatic development and vascular changes, both to characterize tumor dynamics during growth for application in diagnostic and prognostic imaging, and to aid in the development of new therapies by dissecting the effects of treatment. The technical goal for the first year has been to develop a device to image the whole animal by nuclear medicine and optical techniques. Ultimately, we believe that these techniques will be useful in the clinic to detect tumors at small sizes, for lymph node assessment and for the detection of occult metastases.

Optical imaging techniques have been developed for laboratory studies but have recently been extended to humans. SPECT (Single Photon Emission Computed Tomography) is a well accepted clinical tool for which agents and methods exist for the characterization of disease in the clinical environment. The successful translation to the clinic depends upon further advances in crucial technical properties (imaging characteristics, sensitivity and specificity). We specifically propose to study how the dual modality images could be useful in tumor detection and treatment.

We report first our initial results in tomographic imaging of light emission. We present images showing that it is possible to detect small lesions not only subcutaneously but also at depth in vivo, and characterize the advantages of this method for quantitative imaging.

We have also demonstrated micro-SPECT (Single Photon Emission Computed Tomography) imaging at high resolution. We report here on our initial progress in SPECT, and on the advantages of tomography initially for small animals, showing submillimeter resolution in a mouse when imaging bone.

15. SUBJECT TERMS
SPECT, Optical Bioluminescence Imaging, Metastatic Development, Tumor Heterogeneity

16. SECURITY CLASSIFICATION OF:			17. LIMITATION OF ABSTRACT	18. NUMBER OF PAGES	19a. NAME OF RESPONSIBLE PERSON
a. REPORT	b. ABSTRACT	c. THIS PAGE			USAMRMC
U	U	U	UU	39	19b. TELEPHONE NUMBER *(include area code)*

Table of Contents

Cover.....1

SF 298.....2

Introduction.....4

Body.....4-13

Key Research Accomplishments.....14

Reportable Outcomes.....14-17

Conclusions.....18

References.....18-21

Appendices.....21-39

Introduction

The goal of this research project is to investigate the relationship between primary breast tumor vascular development and metastatic potential. To facilitate this research in an in vivo mouse model, we have developed a novel dual modality system for small animal imaging. A high sensitivity optical imaging component is used to detect bioluminescent light emitted from implanted tumor cells that have previous been transfected with the luciferase gene. In the same instrument, these high-sensitivity cameras can be coupled with scintillators and collimators to allow Single Photon Emission Computed Tomography imaging. While the bioluminescent component will be sensitive to the detection of distant metastases, the nuclear medicine aspect of the system will be utilized in subsequent years for studying tumor angiogenesis and vasculature.

Body

Our statement of work specified that the first year would be dedicated to the development of a fully integrated multi-head optical/BLI and micro-SPECT system. Task 1 was subdivided into 8 steps, 1-h. In summary:

a- Gantry and camera housings have been designed, built and tested .
b- Camera and support motion assemblies were built.
c- The CCDs and associated first generation optical/scintillator components were built and tested.
d- The data acquisition system has been completed and assembled with the above components. These have been used with a test optical imaging system based on SITe CCD chips, now completed and in use.
e- The 5-head system was constructed, but we experienced CCD chip failure. As explained below, this caused us to move to a new CCD assembly, with the same price but different characteristics. This required a redesign of the electronics, still in progress.
f- Single camera tests were successful, showing high sensitivity.
g- Development of optical MLEM reconstruction software has progressed, and we have reported our first results in tomographic imaging of light emission. Our images show that it is possible to detect small lesions not only subcutaneously but also at depth in vivo, and we characterizef the advantages of this method for quantitative imaging. 3D images were obtained and reported at the ERA of HOPE symposium.
h- Phantom testing has been completed including both homogeneous, cylindrical, and heterogeneous, mouse-shaped phantoms. We have also demonstrated micro-SPECT (Single Photon Emission Computed Tomography) imaging at high resolution.

We report below on our progress along these points. While the completion of an integrated optical/microSPECT imaging device was temporarily hampered by the commercial failure of the SITe manufacturer, we selected new CCDs with equivalent or better performance. The completion of the new electronics is now advanced. Because of the new features, we expect that the new device will result in portable devices suitable for human applications at a later time.

High Sensitivity CCD camera (a-f)

The dual optical/SPECT imaging system uses CCD (charge-coupled device) cameras selected for their high and nearly constant sensitivity over the full range of wavelengths commonly used in optical imaging, from blue to near infrared. Based on our design the required parameters of the CCD are: non-color, back-illuminated, full frame image sensor, 512x512 pixels, with large pixel size to provide good dynamic range. Preferably the quantum efficiency of the CCD should be greater than 85% from 400 nm to 750 nm, and should remain above 50% up to 900 nm. The originally selected CCD SI-032AB produced by Scientific Imaging Technologies Inc., Tigard, OR fulfilled all this requirements but it is no longer available due to the company's bankruptcy.

Thus, a new CCD was selected, CCD77-00 (e2v technologies, inc. 4 Westchester Plaza, PO Box 1482, Elmsford, NY10523-1482 USA). This CCD has a pixel size of 24x24 μm providing a large well capacity of 300,000 e^-, with a sensitivity of 2.5 μV/e^-, low dark current (20 pA/cm^2 at 20 °C), and low readout noise (3 e^- RMS) providing a dynamic range of ~100,000. The CCD is cooled to -40° C reducing the dark current signal to less than 0.1 e^-/pixel/sec. All relevant parameters are similar or better than those of SI-032AB, but the support electronics requires significant changes. We are currently implementing the new driving circuits (Fig.1) which can provide the new control sequence and voltages.

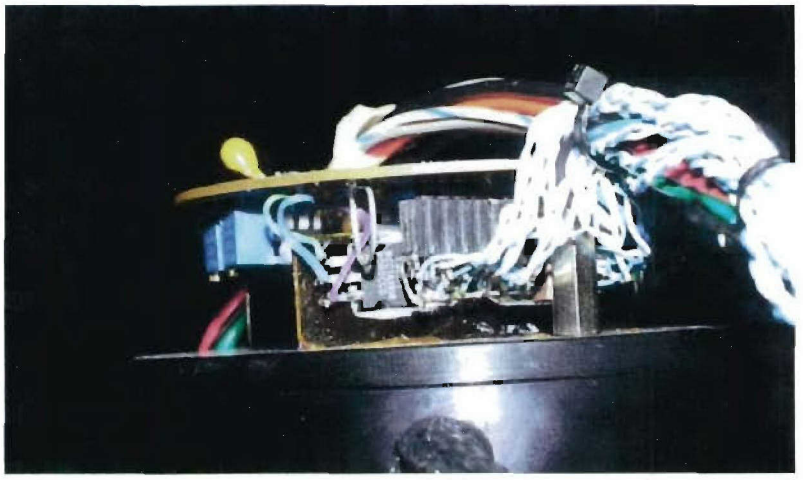

Figure 1. The implemented electronic circuitry for driving the CCD signals.

The CCD is incorporated in a self-contained, cooled camera, equipped with electronic circuitry and fast optics (25 mm focal length, f/0.95). Each camera is calibrated using a low-intensity, diffuse, flat field source that gives a known radiance (typically 3.0 x 10^{-7} W/cm^2/sr). The light source is periodically checked for uniformity using a NIST-traceable research radiometer (model IL 1700, International Light, Inc. Newburyport, MA). By imaging this source the digital units provided by the camera digitizer can be converted directly into absolute physical units (W/cm^2/sr or photons/sec/cm^2/sr). This method accounts for the transmission efficiency of the entire optical system, and corrects the non-uniformity in the field of view due to lens vignetting and variations in pixel sensitivity.

Multiple Head Optical Imaging System

Multiple high sensitivity CCD cameras simultaneously record views, and a computer controlled rotation mechanism, allows imaging at multiple angular positions, as required for three dimensional reconstructions. The support electronics allow simultaneous control of the cameras for light exposure, image readout and preprocessing, and temperature and vacuum control. A horizontal bed, made of sparse mesh material to reduce interference with light, is used to support and immobilize the animal during imaging. A gas anesthesia unit is connected to the bed and to the animal. To exclude ambient light, the system is encapsulated in a light-tight enclosure. Light images at each position of the gantry are acquired for co-registration with the bioluminescence image using a set of 6 diffuse light sources.

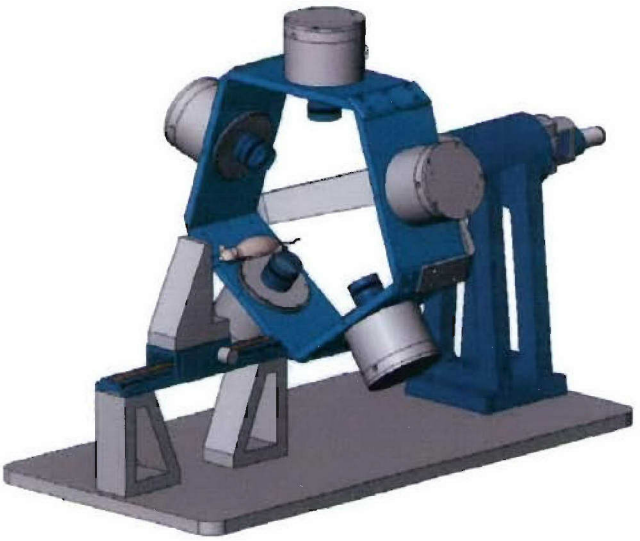

Figure 2. The design of the imaging system includes 5 high sensitivity cameras mounted on a rotating gantry, and a transparent animal positioning system.

Validation studies using phantoms verified the utility of the approach and accuracy of the 3D reconstruction algorithms. Here we describe only two phantoms of increasing complexity, a homogeneous diffusing cylinder and a homogeneous mouse-shaped phantom.

Homogeneous cylindrical phantom (h)

Figure 3a shows the experimental setup with a 30 mm diameter cylindrical phantom filled with 1 % Intralipid / 1% Agarose gel (Intralipid gel for brevity), which approximates light scattering in tissues. An optical fiber (1 mm diameter) was placed in the phantom before congealing the filling mixture and was optically coupled to a 560nm LED. A set of 20 images was obtained for each experiment by rotating the phantom 18° at a time.

The total amount of light captured at each imaging angle both in air and Intralipid phantom is presented in Figure 3b, obtained while keeping the light source intensity constant. The fiber optic source in air shows a small variation due to changes in distance from the lens. When the source was immersed in Intralipid it was noted that for angles between 0 and 180°, when the light source is

closest to the camera, up to 4 times more light was captured than for the source in air, as the scattering of light in the phantom caused a significant increase in the photon flux toward the objective. When the source was in the position furthest from the camera (270°) only half as much light was captured because the light source was shadowed by the body of the phantom. Overall, a variability of almost an order of magnitude was observed when imaging this phantom at different angles, reducing the precision and reliability of a quantitative assessment from single planar images. This effect would be expected to affect animal studies, when light is emitted at depth within the body from multiple sources, such as small metastatic tumors in the lungs or other internal organs.

Figures 3c and 3d show images obtained first in air and then in gel, with the fiber displaced 10 mm from the center at a viewing angle of 180°. A cross-section through the reconstructed 3D image is also shown for each case. The position of the source was correctly identified by the reconstruction algorithm. The total light signal in air and Intralipid differed by only 3% (1,435 x 10^7 photons/sec for air vs. 1,390 x 10^7 photons/sec for Intralipid), further showing the quantitative nature of the 3D reconstruction algorithm in the presence of diffusion. Confirmatory results were also obtained for multiple light sources, both in air and Intralipid, e.g., for two sources separated in depth by 10 mm (Fig. 3e).

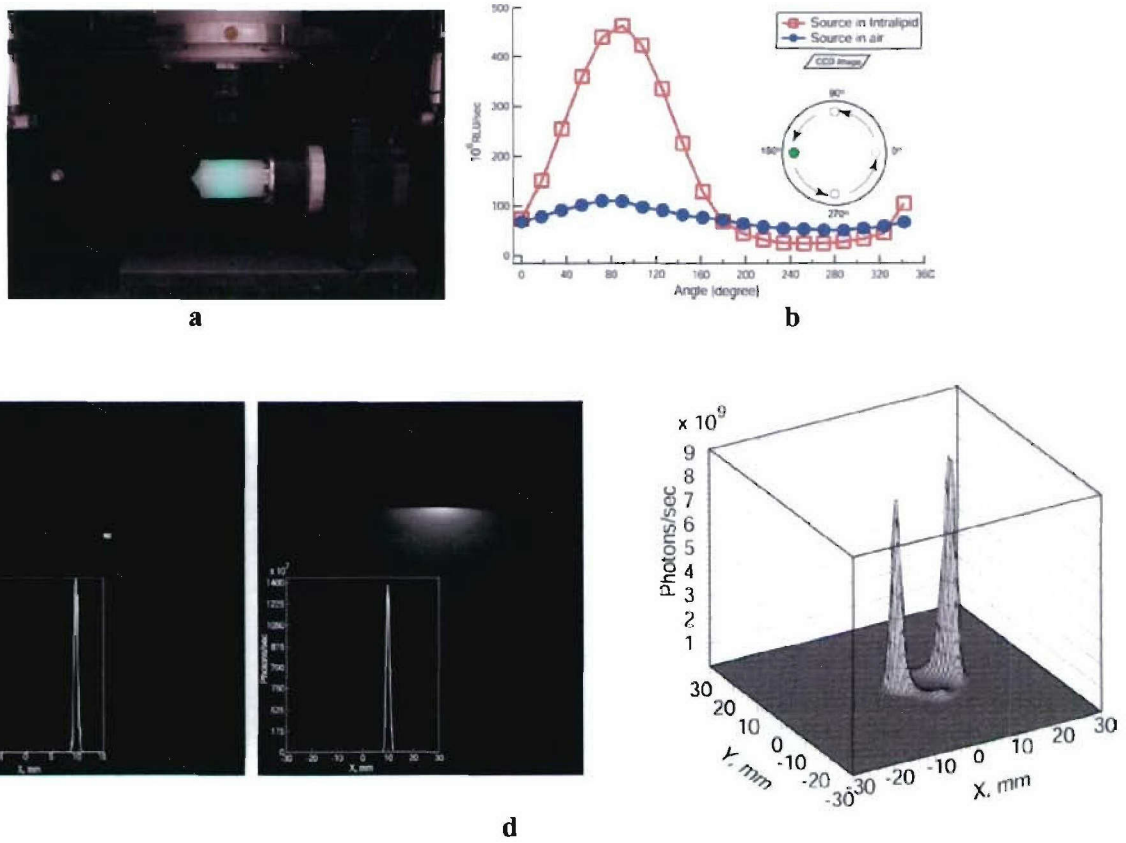

Figure 3. Validation of LET in phantoms.
a. Experimental setup: 30 mm cylindrical phantom filled with 1% Intralipid gel.
b. Total amount of light captured from a fiber optic source in air and in the phantom at various angles. The light source is displaced 10 mm from the axis of rotation.

c, d. Image of light emitting fiber in air (c) and in intralipid-filled medium (d) displaced 10 mm from the center. The intensity profiles through the reconstructed 3D image are also shown.

e. 3D intensity profiles for 1% Intralipid phantom with two sources separated by 10 mm.

Homogeneous mouse shaped phantom

In order to investigate the LET reconstruction in the context of a complex body surface, a mouse shaped 1% Intralipid gel phantom with a 9.5 mm diffuse spherical light source embedded in the thoracic region was completed and imaged on the LET system. Figure 4 shows a longitudinal section of the phantom with the 3D reconstructed source overlay. The reconstructed source is 10 mm in size, in agreement with its physical dimensions, and at the correct location (within 1mm).

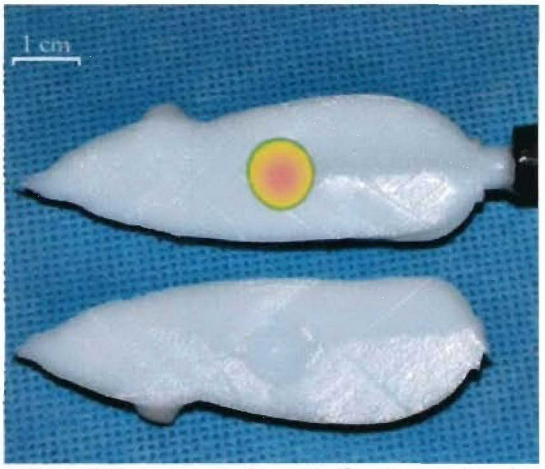

Figure 4. Longitudinal section of the mouse shaped phantom with the 3D reconstructed source overlay.

Optical MLEM Software (f)

Three-Dimensional Bioluminescent Imaging (3D-BLI) of luciferase-expressing cells in live small animals would greatly enhance applications in biomedicine since light emitting cell populations could be unambiguously associated with specific organs or tissues. We consider this pivotal for investigating tumor growth, metastasis, and specific biological molecular events. The imaging approach must account for the main optical properties of biological tissue because light emission from a distribution of sources at depth is strongly attenuated due to optical absorption and scattering in tissue. Our image reconstruction method is based on the deblurring Expectation Maximization (EM) method and takes into account both of these effects. To determinate the boundary of the object (skin surface), we use the standard iterative algorithm - Maximum Likelihood (ML) reconstruction method. Depth-dependent corrections for quantitative light intensity were included in the reconstruction procedure by using the diffusion equation for light transport in semi-infinite turbid media with extrapolated boundary conditions.

For detection of bioluminescence emitting probes in living animals, it is necessary to use high sensitivity low-noise detectors, such as cooled Charged-Coupled Devices (CCDs), and advanced software codes for image reconstruction. Reconstruction algorithms must take into

account the main optical properties of biological tissue: light absorption, scattering, and possibly reflection at major interfaces. In this case, a model describing light transport in turbid media is critical for any reconstruction technique[15]. Widely used methods include the Monte Carlo approach[16-19] and the Radiative Transfer Equation (RTE) [20-24].

The Monte Carlo method is a discrete model of individual photon interactions that can be described by computer simulation of appropriately weighted random absorption and scattering events. This method is an accurate and powerful way to study photon transport in tissue requiring no simplifications, but expensive computational resources are often needed due to the slow statistical nature of the method.

The RTE method is a continuous model based on an integro-differential equation, specifically a Boltzman-like transport equation for the photon wave intensity, which includes emission, absorption, and scattering in the media. This equation most often can not be solved analytically, and is often simplified by a diffusion approximation[20] for numerical solution. The diffusion equation gives us not only a great simplification of the problem but a practical tool to describe the diffuse part of the radiative intensity. A disadvantage of this method is the inaccuracy in predicting the light distribution near light sources and boundaries. The diffusion approximation is only valid for materials where scattering dominates over absorption.

FORWARD MODEL: LIGHT DIFFUSION IN TURBID MEDIA

To determine the position of bioluminescence sources we must describe photon propagation through tissue (light can be considered as a stream of photons) and simplify the RTE to the diffusion approximation. The RTE is an integro-differential equation derived by considering energy conservation in a small volume dV. The photon distribution function $N(\mathbf{r}, \hat{s}, t)$ depends on time t and can be spatially-varying with any position $\mathbf{r}$ (x, y, z) in direction $\hat{s}(\theta, \varphi)$. $L(\mathbf{r}, \hat{s}, t) = c\, h\nu\, N(\mathbf{r}, \hat{s}, t)$ is the radiance - power per unit area per unit solid angle Ω, h is the Planck constant, ν is photon frequency, and c is photon speed in vacuum. Photons can only be added or subtracted from the photon distribution function if they interact in this volume dV through the following processes[20]: i) photons are lost through the boundary of media with different refraction index n; ii) photons incoming in direction $\hat{s}$ can be absorbed with absorption coefficient $\mu_a(\mathbf{r})$ or scattered to any another direction $\hat{s}'$ with scattering coefficient $\mu_s(\mathbf{r})$ and a probability (phase function) $\rho(\hat{s}, \hat{s}')$; iii) photons can be gained through scattering from any direction $\hat{s}'$ into the direction $\hat{s}$; iv) photons are also gained through an internal light source $S(\mathbf{r}, \hat{s}, t)$.

If we neglect interference effects of photons and drop the integrals over volume, we can write the time-dependent RTE for the radiance:

$$\frac{1}{c_n}\frac{\partial L(r,\hat{s},t)}{\partial t} = -\hat{s}\nabla L(r,\hat{s},t) - \mu_a L(r,\hat{s},t) - \mu_s L(r,\hat{s},t)$$
$$+ \mu_s \iint_{4\pi} \rho(\hat{s},\hat{s}') L(r,\hat{s},t) d\Omega' + S(r,\hat{s},t) \qquad (1)$$

where $c_n = c/n$ is the speed of light in the tissue.

By applying the P1 expansion approximation and assuming that the scattering coefficient dominates the absorption coefficient, the RTE can be further simplified to a time-dependent diffusion equation:

$$\frac{1}{c_n}\frac{\partial\phi(r,t)}{\partial t} = -D\nabla^2\phi(r,t) - \mu_a\varphi(r,t) + S(r,t) \qquad (4)$$

The analytic solution for an isotropic point-like source $S(r,t) = \delta(r,t)$ is the time-domain Green's function:

$$G(r,t) = c_n(4\pi Dc_n)^{-3/2} e^{-\mu_a c_n t} e^{-r^2/4\pi c_n t} \qquad (5)$$

and the solution to the diffusion equation (4) for radiance is given by the convolution:

$$\varphi(r,t) = G(r,t) \otimes \delta(r,t) \qquad (6)$$

For steady-state diffusion, as is the case with BLI, we can neglect the time-dependence in equation (4) and obtain:

$$\varphi(r) = S_0 e^{-\mu_{eff} r} \frac{(4\pi D)^{-1}}{r} \qquad (7)$$

where the source power S_0 is constant in amplitude, and the radiance decreases exponentially with distance **r**, according to an effective attenuation coefficient $\mu_{eff} = (\mu_a / D)^{1/2}$.

The next problem is the refraction of photons at the tissue-air interface that will reduce the fluence rate out of the animal. We have adopted the solution for semi-infinite medium with extrapolated boundary and photon dipole source model [2,31–34] and used it to quantify the light intensity from experimental data for phantom filled with Intralipid [35]. This diffusion solution has been shown to be in good agreement with Monte Carlo simulations and experiments [2,31,34].

The diffusion approximation is very useful for estimating the surface photon intensity and spot size depth-dependence for BLI experiments, especially for in vivo small animal studies. Figure 5 shows surface radiance and its spot size as a function of depth for different tissue optical parameters. The distributions for the absorption surface intensity for several sets of absorption coefficients are plotted in Fig.1a, while the surface intensity for variable scattering coefficients is plotted in Fig.1b. Figure1c shows the parameter Full Width Half Maximum (spot size) for different concentration of Intralipid: higher concentrations of Intralipid give lower photon intensity level, but spatial resolution is better for depths ~1-1.5 cm. This depth is consistent for good results for small animal BLI reconstruction.

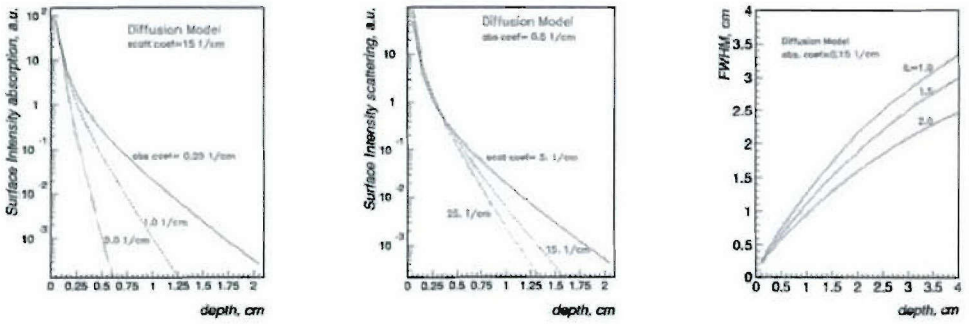

a **b** **c**

Fig.5 Surface Intensity Peak (a)-(b) and FWHM (c) as a function of source depth calculated for different concentration of Intralipid by diffusion approximation with extrapolated boundary condition.

Now we can calculate distributions of surface intensity for two sources with some separation as a function of source depth. As shown in Fig.6 intensity decreases with depth, and at more than 12 mm depth the two peaks are practically inseparable. In this case, reconstruction of two sources becomes problematic.

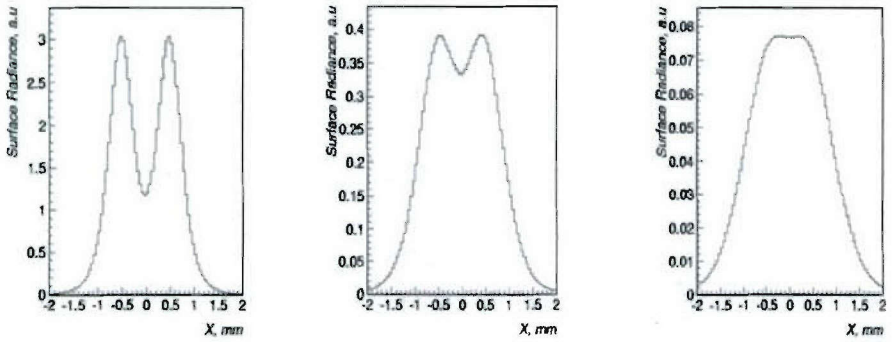

a **b** **c**

Fig.6 Surface Intensity for two sources with separation 10 mm as a function of depth: a) 4 mm, b) 8 mm and c) 12 mm for 1% Intralipid concentration.

IMAGE RECONSTRUCTION METHODS

We have developed a 3-D reconstruction algorithm for small animal imaging, and this paper presents the results for reconstruction in the multi-scattering, continuous wave regime. By using detectors with constant response over the entire range of wavelengths expected for the light-emission problem at hand, our images are proportional to the number of quanta captured in each pixel. Our reconstruction approach consists of two steps: light surface reconstruction to determine the geometry of turbid media boundary followed by source reconstruction inside the tissue.

The surface reconstruction is based on the ML method [40-41]. Using the ML algorithm, a sequence of image estimates is generated for the k^{th} iteration:

$$n_j^{k+1} = \frac{n_j^k}{\sum_{i=1}^{I} a_{ij}} \sum_{i=1}^{I} \frac{m_i}{q_i^k} \quad \text{where} \quad q_i^k = \sum_{j=1}^{J} a_{ij} n_j^k \tag{12}$$

where n_j^{k+1} and n_j^k are image intensity values in the new and current estimate for the voxel j. The measured data m_i collected along lines i which connect a voxel on the object's surface to the CCD camera, gave values proportional to the light intensity detected by the pixel; q_i^k is the expected count in line i for the current estimate n^k, and a_{ij} is the probability that a light quantum emitted at voxel j will be detected in the line i. The normalization factor $\sum_{i=1}^{I} a_{ij}$ includes all possible measured lines. Figure 7 shows examples of ML surface reconstruction for the phantom with two interior sources and for an externally illuminated living mouse.

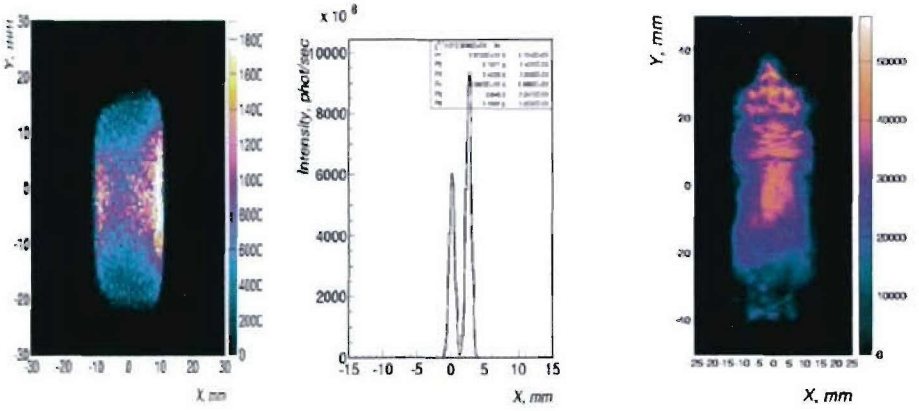

a b c

Fig.7 Surface reconstruction by ML method for phantom with two interior sources (a), 3D-reconstruction for sources in air with separation 2.52 mm (b) and 3D surface (skin) reconstruction of nude mouse from reflected light (c).

The volumetric reconstruction of the source is a very important part of LET, and this problem is formulated as an inverse source problem based on diffusion approximation [42–44]. The solution uniqueness for BLI reconstruction can be assured by incorporation of a priori information on the animal anatomy and optical properties [24,45–47]. Good results for 3D- optical reconstruction have also been obtained by using the Finite Element Method [48–52]. In [50] two sources with ~10 mm separation were reconstructed using an FEM algorithm. We will show below our reconstruction results for the same separation.

We present another technique – the iterative deblurring EM method [53–55] based on diffusion approximation. In our approach good reconstruction can be obtained if the sources intensities on the surface permit some separation (see Fig.6). Our experimental data in this case for backprojection onto x –axis follows this (see Fig. 8), and we expect a good reconstruction.

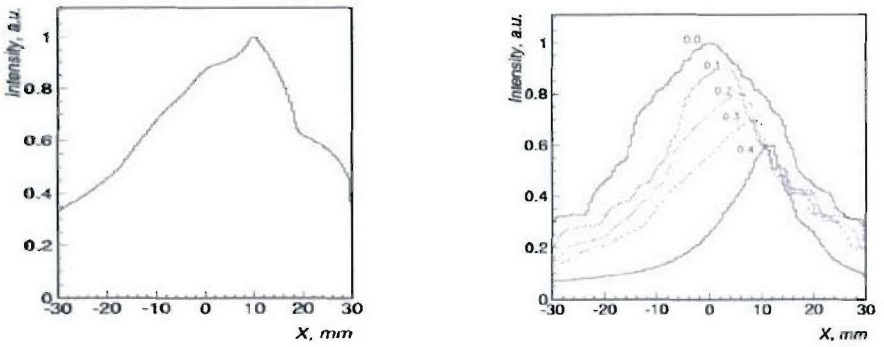

a b

Fig.8 Backprojection histograms for 1% Intralipid phantom with two sources located in 0 mm and 10.16 mm (a) and for phantoms with different source positions on x-axis in inches (b). On y- and z-axis sources located in 0 mm position for each phantom. Voxel size = 0.5 mm.

We can take into account reflection on boundary[33-37] estimate values for each voxel, and subtract this reflection contribution. Next for each voxel we can determine a "zero-th" order approximation (i.e. initial guess as a input image) using the solution for point source photon flux:

$$\varphi_j^0 = (\rho \otimes \varphi + \hat{n})_j \cong \frac{1}{\sum_{i=1}^{I} x_{ij} p_i'} \sum_{i=1}^{I} x_{ij} p_i^0 \sum_{s=1}^{s=S} \exp(-\mu_{eff} r_{js}) / r_{js} \qquad (13)$$

where ρ is a point-spread function, φ is a real value of photon flux, $\hat{n}$ is a noise term, and x_{ij} is the path length of line i through voxel j, p_i' and p_i^0 are intensities in CCDs from source in media and in air, and S is number of sources. After correcting all voxels for boundary conditions we apply the deblurring EM algorithm for 3D-image reconstruction:

$$\varphi_j^{n+1} = \varphi_j^n \left\{ \hat{\rho} \otimes \left(\frac{\varphi_j^0}{\rho \otimes \varphi_j^n} \right) \right\} \qquad (14)$$

where $\otimes$ denotes convolution procedure based on the discrete Fast Fourier Transform[56]. Parameters ρ and $\hat{\rho}$ are the deblurring kernels (for example Gaussian functions) and can be changed with number of iterations n.

Key Research Accomplishments

- Gantry and camera housings have been designed, built and tested .
- Camera and support motion assemblies were built.
- The CCDs and associated first generation optical/scintillator components were built and tested.
- The data acquisition system has been completed and assembled with the above components. These have been used with a test optical imaging system based on SITe CCD chips, now completed and in use.
- The 5-head system was constructed, but we experienced CCD chip failure. As explained below, this caused us to move to a new CCD assembly, with the same price but different characteristics. This required a redesign of the electronics, still in progress.
- Single camera tests were successful, showing high sensitivity.
- Development of optical MLEM reconstruction software has progressed, and we have reported our first results in tomographic imaging of light emission. Our images show that it is possible to detect small lesions not only subcutaneously but also at depth in vivo, and we characterizef the advantages of this method for quantitative imaging. 3D images were obtained and reported at the ERA of HOPE symposium.
- Phantom testing has been completed including both homogeneous, cylindrical, and heterogeneous, mouse-shaped phantoms. We have also demonstrated micro-SPECT (Single Photon Emission Computed Tomography) imaging at high resolution.

Reportable Outcomes

1) ERA of HOPE abstract P64-3

INVESTIGATION OF METASTATIC BREAST TUMOR HETEROGENEITY AND PROGRESSION USING DUAL OPTICAL/SPECT IMAGING

Peter P. Antich, Matthew A. Lewis, Edmond Richer, Nikolai Slavine, Todd Soesbe, Xiufeng Li, Anca Constantinescu, Allen Harper, Ralph P. Mason

The immediate goal of our project is to image tumor growth, metastatic development and vascular changes, both to characterize tumor dynamics during growth for application in diagnostic and prognostic imaging, and to aid in the development of new therapies by dissecting the effects of treatment. More specifically, our technical goal for the first year is to develop he device necessary to image by nuclear medicine and optical techniques. We have begun assembling the physical and biological components of our research.

Optical imaging techniques have been developed to characterize cells and molecules in the laboratory. They are currently used with microscope techniques in excised tissues or living cells. They are now being extended to the analysis of biologic phenomena in living mammalian organisms and have found a strong application in drug screening. Their first applications to noninvasive human studies are envisaged in the detection of oxygen saturation. We are interested in advancing this technology to obtain, e.g., oxygen-dependent 3D images. The successful translation to the clinic depends upon a crucial question – can small lesions be detected at depth or is this method limited to contact or

small distance imaging? We had previously completed a three-dimensional imager of light emitted via bioluminescence both in its hardware and image reconstruction software. We report here on initial results in tomographic imaging of light emission. We present images showing that it is possible to detect small lesions not only subcutaneously but also at depth in the mouse lungs and viscera, and characterize the advantages of this method for quantitative imaging.

We have also demonstrated micro-SPECT imaging of bone, in order to assess our ability to detect vascular phenomena and bone metastases at high resolution. Nuclear medicine is a well accepted clinical tool, for which agents and methods exist reportedly able to detect and potentially stage disease in the clinical environment. We report here on our initial progress in SPECT, and on the advantages of tomography initially for small animals, showing submillimeter resolution in a mouse when imaging bone. This form of imaging may be used to detect bone metastases. **POSTER ATTACHED**

2)

NOVEL APPLICATION OF BIOLUMINESCENT IMAGING: INTERROGATING ACUTE EFFECTS OF THE VASCULAR TARGETING AGENT COMBRETASTATIN.

Dawen Zhao, Allen Harper, Edmond Richer, Li Liu, Nikolai Slavine, Jerry W. Shay, Peter P. Antich and Ralph P. Mason
Cancer Imaging Program, Department of Radiology and Cell Biology, UT Southwestern, Dallas, TX, USA 75390

Vascular targeting agents promise therapeutic efficacy by selectively cutting of the blood supply to tumors inducing massive cell death. Combretastatin (CA4P) represents a lead drug and is in advanced clinical trials. Numerous reports indicate acute changes in perfusion observed by MRI reporting rapid vascular shutdown in tumors. We recently measured acute hypoxiation within 90 mins following CA4P administration to rats with breast tumors using ^{19}F MRI oximetry (Zhao *et al.*, *IJROBP* 2005). We have now applied BLI to probe the acute effects of CA4P on human breast 231 adenocarcinomas transected to stably express luciferase.

231 cells were transfected with lentivirus to express luciferase and highly expressing clones isolated. 10^6 cells were implanted in the flank of nude mice and allowed to grow to ~ 6 mm diameter. Sty this stage mice were anesthetized (isoflurane/O_2). A solution of luciferin-D (sodium salt 450 mg/kg) was administered SC in the neck region and light images acquired immediately using one camera of our Light Emission Tomography System (LETS). Serial images (30 s each) were acquired over a period of 20 – 30 mins and the light intensity – time curves evaluated. Saline or CA4P in saline (120 mg/kg) were injected IP immediately after baseline BLI and then 2 h and 24 h later the BLI time course was repeated. We also undertook 3D imaging by acquiring multiple images simultaneously using 3 cameras arranged in a circular gantry around the mouse. Data were reconstructed using a statistical MLEM approach and deconvolution to provide fully 3D images.

Control tumors showed intense light emission peaking within 8 mins and generally decreasing to about 50-70% after 20 mins. Repeat measurements after saline infusion essentially indicated similar kinetics. By contrast, CA4P led to a significantly lower light

emission (peak ~ 2 to 10 times lower) and delayed peak emission. 24 h later signal remained considerably decreased. Traditional BLI provides a planar image only, but tumors are 3D and known to exhibit heterogeneity particularly after vascular targeting agents. LETS was successful providing 3D representation of the tumors.

While BLI has been reported extensively in terms of measuring tumor burden with respect to growth and response to therapy, we believe that application to examine acute effects of vascular targeting agents is a novel application. It can provide a cheap high throughput method for evaluating novel drugs and drug combinations and scheduling.

Supported by the NCI Cancer Imaging Program pre-ICMIC CA86354, DOD Breast Cancer Initiative (DAMD 170310363) (DZ) and Simmons Cancer Center.

3) University of Texas Molecular Medicine Symposium Invited Speaker

Three-Dimensional Imaging of Cellular and Molecular Events in the Living Animal by Light Emission Tomography

The emerging field of *in vivo "molecular imaging"* encompasses a diverse array of noninvasive imaging methods which enable gene expression and other molecular biology assays to be detected and visualized in living animals Cell assays have been developed to study genetic regulatory elements, protein trafficking and protein function. Extension of this type of analysis to intact living animals, and eventually translation to humans, will enhance our understanding of gene regulation and protein function in functional tissues and organs. Molecular imaging is now performed with MRI, PET, SPECT and CT, as well as by the latest light emission imaging techniques, in particular bioluminescence and fluorescence imaging.

When sets of images obtained by different techniques, or different reporter molecules, measure and display different properties, it is of great interest to analyze their interrelation. To do so, it is preferable to achieve spatio-temporal coregistration of data sets obtained with the different methods. To this end, molecular imaging methods should preferably be three-dimensional and also quantitative, so that the data extracted from its images can be used to reveal mechanisms through which the biological processes unfold.

This talk focuses on techniques and methods to perform quantitative, three-dimensional bioluminescent imaging (BLI). The technique is based on transfection of the luciferase gene (North American firefly, *Photinus pyralis*), which is readily introduced into diverse cell lines with selection for most effective expression. When D-luciferin is administered to the cells or to an animal host, a bioluminescent reaction emits light that can be detected. Our current research focus is on imaging the evolution and treatment of primary tumors and distant metastases. Detection of metastatic foci, study of the dynamics of metastatic development, and study of response to therapy of primary tumor and metastatic foci are tasks which demand high sensitivity and resolution in the context of noninvasive whole-body imaging,.

To date, BLI has been mostly limited to a planar technique, where the effectiveness of the 2D method is restricted in terms of localization of cell population (visualization at depth) and size estimation (quantitation of tumor burden and progression). Due to light scattering and absorption, 3-D reconstruction of light emission from a source at depth poses major difficulties. The intensity and spatial distribution of the BLI signal are strongly influenced by

the intervening tissues, which can be accounted for numerically if the anatomic distribution of tissues and their optical properties are known.

Here, we describe an imaging method to accomplish this task, light emission tomography (LET), obtained by applying to data obtained all around the mouse an algorithm based on image reconstruction techniques well-established for single-photon emission tomography, but differing in dynamic factors which account for photon absorption and diffusion. The reconstruction method is validated in simple phantoms of appropriate dimensions, showing its ability to overcome diffusion effects and to achieve optimal quantitative power. Representative images obtained in living animals are shown to document the ability of the method to image small lesions at depth.

In summary, three-dimensional (3D) optical imaging of bioluminescence has the potential to provide unique insight into tumor development and metastasis. Compared to planar BLI, it enhances sensitivity and detectability. The method permits a quantitative assessment of cancer cell burden in living animals, providing information both on cell numbers and, combined with anatomical information, their localization in organs.

4)

Richer E, Slavine N, Lewis MA, Tsyganov E, Gellert GC, Dikmen ZG, Bhagwandin V, Shay JW, Mason RP, Antich PP: Three Dimensional Light Emission Tomography using Multiple Rotating CCD Cameras. Third Annual Meeting of The Society for Molecular Imaging, 9-12 September, 2004, St. Louis. **POSTER ATTACHED**

5)

Richer E, Lewis MA, Smith B, Li X, Seliounine S, Mason RP, Antich PP: Comparison of CsI(Tl) and Scintillating Plastic in a Multi-Pinhole/CCD-based Gamma Camera for Small Animal Low Energy SPECT. Small-animal SPECT Imaging: Proceedings of The University of Arizona Center for Gamma-Ray Imaging Workshop on Small-Animal SPECT, Chapter 13, Springer-Verlag, 2005. **PREPRINT ATTACHED**

6)

Lewis MA, Arbique G, Richer E, Slavine N, Jennewein M, Constantinescu A, Brekken R, Guild J, Tsyganov EN, Mason RP, Antich PP: Projection and pinhole based data acquisition for small animal SPECT using storage phosphor technology. Small-animal SPECT Imaging: Proceedings of The University of Arizona Center for Gamma-Ray Imaging Workshop on Small-Animal SPECT, Chapter 26, Springer-Verlag, 2005. **PREPRINT ATTACHED**

7)

Z.G. Dikmen, G. Gellert, P. Dogan, R. Mason, P. Antich, E. Richer, W.E. Wright, J.W. Shay, " A New Diagnostic System in Cancer Research: Bioluminescent Imaging", Turk. J. Med. Sci. **35**, 65-70 (2005).

8)

PAROO Z, BOLLINGER RA, BRAASCH DA, RICHER E, COREY DR, ANTICH PP, MASON RP (2004) VALIDATING BIOLUMINESCENCE IMAGING AS A HIGH-THROUGHPUT, QUANTITATIVE MODALITY FOR ASSESING TUMOR BURDEN. MOLECULAR IMAGING 3(2):117-124.

Conclusions

Successful completion of the instrument development specific aims in Year 1 will allow the initiation of experiments in the animal model that were proposed in Year 2. Initial imaging experiments in tumor-bearing mice are in progress at present.

References

[1] C.H. Contag, P.R. Contag, J.I. Mullins, S.D. Spilman, D.K. Stevenson, D.A. Benaron, "Photonic detection of bacterial pathogens in living hosts", Mol. Microbiol, **8**, 593-603 (1995).

[2] B.W. Rice, M.D. Cable, M.B. Nelson, "In vivo imaging of light-emitting probes", J.Biomed.Opt. **6**, 432-440 (2001).

[3] S. Bhaumik, S.S. Gambhir, "Optical imaging of Renilla luciferase reporter gene expression in living mice", PNAS, **99**, 377-382 (2002).

[4] C.H. Contag, M.N. Bachmann, "Advances in Bioluminescence imaging of gene expression", Annu. Rev. Biomed.Eng. **4**, 235-260 (2002).

[5] S.H. Thorne, C.H. Contag, "Using In Vivo Bioluminescence Imaging to Shed Light on Cancer Biology", Proc. IEEE, **93**, 750-762 (2005).

[6] T.F. Massound, S.S. Gambhir, "Molecular Imaging in living subjects: Seeing fundamental biological processes in a new light", Genes and development **17**, 545-580 (2003).

[7] R. Blasberg, " In vivo molecular-genetic imaging: multi-modality nuclear and optical combinations", Nucl. Med. Biol. **30**, 879-888 (2003).

[8] S.R. Cherry, "In vivo molecular and genomic imaging: new challenges for imaging physics", Phys. Med. Biol. **49**, R13-R48 (2004).

[9] A. Chatziioannou, "In-Vivo Optical Imaging: principles and Technology", M248: Introduction to Biological Imaging, UCLA, Crump Inst. for Molecular Imaging, January 27 (2004).

[10] V. Ntziachristos, J.Ripoll, L.Wang, R. Weissleder, "Looking and Listening to light: the evolution of whole-body photonic imaging", Nat. Biotech. **23**, 313-320 (2005).

[11] Z. Paroo, R.A. Bollinger, D.A. Braasch, E. Richer, D.R. Corey, P.P. Antich, R.P. Mason, "Validating Bioluminescence Imaging as a High-Throughput, Quantitative Modality for Assessing Tumor Burden", Molec. Imaging **3**, 1-8 (2004).

[12] C.H. Contag, B.D. Ross, " It's not just about anatomy: in vivo bioluminescence imaging as an eyepiece into biology", J. Magn, Res. Imaging **16**, 378-787 (2002).

[13] Herschman H.R., "Molecular imaging: looking at problems, seeing solutions", Science **302**, 605-608 (2003).

[14] J. Marx, "Building better mouse models for studying cancer", Science **299**, 1972-1975 (2003).

[15] S.R. Arridge, J.C. Hebden, "Optical imaging in medicine: II. Modeling and reconstruction", Phys. Med. Biol. **42**, 841-853 (1997).

[16] B.C. Wilson, G. Adam, "A Monte Carlo model for the absorption and flux distribution of light in tissue", Med. Phys **10**, 824-830 (1983).

[17] S.T. Flock, M.S. Patterson, B.C. Wilson, D.R. Wyman, " Monte Carlo modeling of light propagation in highky scattering tissues – I: Model predictions and Comparison with Diffusion Theory", IEEE Trans. Biol. Eng. **36**, 1162-1168 (1989).

[18] A. Kienle, M.S. Patterson, "Determination of the optical properties of turbid media from a single Monte Carlo simulation", Phys.Med.Biol. **41**, 2221-2227 (1996).

[19] L. Wang, S.L. Jacques, L. Zheng, " MCML – Monte Carlo modeling of light transport in multi-layered tissues", Comp. Meth. and Programs in Biomedicine, **47**, 131-146 (1995).

[20] Akira Ishimaru, "Wave propagation and Scattering in Random Media", IEEE Press, Oxford - New York (1977).

[21] S. Shandrasekhar, "Radiative Transfer", Dover Publ. Inc, New York (1960).

[22] V. Venugopalan, B.J. Tromberg, " Radiative transport in diffusion approximation: an extension for highly absorbing media and small source-detector separations", Phys.Rev. **E58**, 2395-2407 (1998).

[23] A.D. Klose, A.H. Hielsscher, "Fluorescence tomography with simulated data based on the equation of radiative transfer", Optic Letters **28**, 1019-1021 (2003).

[24] Ge Wang, Yi Li, Ming Jiang, "Uniqueness theorems in bioluminescence tomography", Med. Rhys. **31**, 2289-2299 (2004).

[25] V. Ntziachristos, C. Tung, C. Bremer, R. Weissleder, "Fluorescence molecular tomography resolves protease activity in vivo", Nature Med. **8**, 757-760 (2002).

[26] A.H. Hielscher, "Model-based iterative image reconstruction for photon migration tomography", SPIE, **3**, 106-117 (1997).

[27] A.H. Hielscher, A.D. Klose, K.M. Hanson, "Gradient-based Iterative Image reconstruction scheme for Time-resolved Optical tomography", IEEE Trans. on Med. Imaging, **18**, 262-271 (1999).

[28] H. Dehghani, B.A. Brooksby, B.W. Pogue, K.D. Paulsen, "Effects of refractive index on near-infrared tomography of the breast", App. Opt. **44**, 1870-1878 (2005).

[29] E. Richer, N. Slavine, M. Lewis, G.Gellert, Z. Dikmen, V. Bhagwandin, J. Shay, R.P. Mason, P.Antich, " Three Dimensional Light Emission Tomography using multiple rotating CCD Cameras", The Third Ann. Meet. Soc. for Molecular Imaging, St. Louis, USA, 216 (2004).

[30] B.J. Berne and R. Pecora, "Dynamic Light Scattering with applications to Chemistry, Biology and Physics", Dover Publ. Inc, New York (2000).

[31] M.S. Patterson, B. Chance, B.C. Wilson, " Time resolved reflection and tranmittance for the non-invasive measurement of tissue optical properties", Applied Optics **28**, 2331-2336 (1989).

[32] T.J. Farrell, M.S. Patterson, B. Wilson, "A diffusion theory model of spatially resolved, steady-state diffuse reflectance for the non-invasive determination of tissue optical properties in vivo", Med. Phys. **19**, 879-888 (1992).

[33] R.C. Haskell, L.O. Svaasand, Tsong-Tseh Tsay, Ti-Chen Feng, M.S. McAdams, B.J. Tromberg, "Boundary conditions for the diffusion equation in radiative transfer", J. Opt. Soc. Am. **11**, 2727-2741 (1994).

[34] A.H. Hielscher, S.L. Jacquest, L. Wang, F.K. Tittel, "The influence of boundary conditions on the accuracy of diffusion theory in time-resolved reflectance spectroscopy of biological tissue", Phys. Med. Biol. **40**, 1957-1975 (1995).

[35] T.C. Soesbe, N.V. Slavine, E. Richer, P.P. Antich, " A solid tissue phantom for tomographic bioluminescence imaging studies", Radiology Department of the University of Texas Medical Center, Dallas, December 17, 1-13 (2004).

[36] A. Kienle, M.S. Patterson, "Improved solutions of the steady-state and the time-resolved diffusion equations for Reflectance from semi-infinite turbid medium", J. Opt. Soc. Am. **14**, 246-254 (1997).

[37] Wang Lihong, "Rapid modeling of diffusion Reflectance of light in turbid media", J.Opt.Soc.Am. **15**, 936-944 (1998).

[38] G.W. Faris, "Diffusion equation boundary conditions for the interface between turbid media: comment", J. Opt. Soc. Am. **19**, 519-520 (2002).

[39] R. Cubeddu, A. Pifferi, P. Taroni, A. Torricelli, G. Valentini, "A solid tissue phantom for photon migration studies", Phys. Med. Biol. **42**, 1971-1979 (1997).

[40] R.T. Whitaker, J. Gregor, " A Maximum Likelihood Surface Estimator for Dense Range Data", IEEE, Trans. Pattern Analysis and Machine. Intell. **24**, 1372-1387 (2002).

[41] L.A. Shepp, V. Vardi, "Maximum Likelihood Reconstruction for emission tomography", IEEE, Trans. Med. Imaging **1**, 113-122 (1982).

[42] T.J. Connolly, D.J. Wall, "On an Inverse problem, with boundary measurements, for the steady state diffusion equation", Inverse Problem **4**, 995-1012 (1988).

[43] S.R. Arridge, "Optical tomography in medical imaging", Inverse Problem **15**, R41-R93 (1999).

[44] V.A. Merkel, J.C. Schotland, "Inverse scattering for the diffusion equation with general boundary conditions", Phys. Rev. **E64**, 035601(R) (2001).

[45] G. Wang, E.A. Hoffman, G. McLennan, L. Wang, M. Suter, J. Meinel, "Development of the first bioluminescent CT scanner", Radiology **229**(P), N1034, 566 (2003).

[46] W. Cong, D. Kumar, Y. Liu, A. Cong, G. Wang, "A practical method to determine the light source distribution in bioluminescent imaging", Proc. SPIE, August 5 (2004).

[47] M. Schweiger, S.R. Arridge, "Optical tomographic reconstruction in a complex head model using a priori region boundary information", Phys. Med. Biol. **44**, 2703-2721 (1999).

[48] S.R. Arridge, M. Schweiger, M. Hiraoka, D.T. Delpy, "A finite element approach for modeling photon transport in tissue", Med. Phys. **20**, 299-309 (1993).

[49] M. Schweiger, S.R. Arridge, M. Hiraoka, D.T. Delpy, "The finite element method for the propagation of light in scattering media: Boundary and source conditions", Med.Phys. **22**, 1779-1792 (1995).

[50] S.R. Arridge, M. Dehghani, M. Schweiger, E. Okada, "The finite element method for the propagation of light in scattering media: A direct method for domains with nonscatering regions", Med. Phys. **27**, 252-264 (2000).

[51] Xuejun Gu, Qizhi Zhang, L. Larcom, H. Jiang, "Three-dimensional bioluminescence tomography with model-based reconstruction", Optics Expres **12**, 3996-4000 (2004).

[52] M.A. Lewis, N.Slavine, E. Richer, P. Antich, "On the minimally-resolvable separation of two point sources in a cylinder of turbid media", Radiology Department of the University of Texas Medical Center, March 18, 1-6 (2005).

[53] T.J. Holmes, "Blind Deconvolution quantum-limited incoherent imagery: Maximum Likelihood Approach", J. Opt. Soc. Am. **9**, 1052-1061 (1992).

[54] Y.L. You, M. Kaveh, "A regularization approach to join blur identification and image restoration", IEEE Trans. Image Proc. **5**, 416-427 (1996).

[55] Ming Jiang, Ge Wang, M.W. Skinner, J.T. Rubinstein, "Blind Deblurring of spiral CT Images", IEEE Trans. Med. Imaging **22**, 837-845 (2003).

[56] C.S. Burrus, T.W. Parks, "Discrete Fourier Transform, Fast Fourier Transform and Convolution Algorithms", John Wiley and Sons Inc, New York (1984).

[57] M. Firbank, D.T. Delpy, "An improved design for a stable and reproducible phantom material for use in near-infrared spectroscopy and imaging", Phys.Med.Biol. **40**, 955-961 (1995).

[58] Neural Networks, EE048941, "EM Algorithms", Technion, spring (2001).

[59] G.J. McLachlan, T. Krishnan, "The EM Algorithm and Extensions", John Wiley and Sons Inc., New York (1997).

[60] J.M. Park, S.S. Gambhir, "Multimodality Radionuclide, Fluorescence, and Boluminescence Small Animal Imaging", Proc. IEEE **93**, 771-783 (2005).

[61] Z.G. Dikmen, G. Gellert, P. Dogan, R. Mason, P. Antich, E. Richer, W.E. Wright, J.W. Shay, " A New Diagnostic System in Cancer Research: Bioluminescent Imaging", Turk. J. Med. Sci. **35**, 65-70 (2005).

Appendices

Please find attached two book chapters and 2 conference posters mentioned above in Reportable Outcomes.

A Dual Modality Optical/SPECT Imaging System for Murine Models of Human Breast Cancer

Peter P. Antich, Matthew A. Lewis, Edmond Richer, Nikolai Slavine, Ralph P. Mason, Dawen Zhao, Todd Soesbe, Xiufeng Li, Anca Constantinescu
Advanced Radiological Sciences, Department of Radiology, The University of Texas Southwestern Medical Center at Dallas

Abstract

The goal of our project is to image tumor growth, metastatic development and vascular changes, both to characterize tumor dynamics during growth for application in diagnostic and prognostic imaging, and to aid in the development of new therapies by dissecting the effects of treatment. The technical goal for the first year has been to develop a device to image the whole animal by nuclear medicine and optical techniques. Ultimately, we believe that these techniques will be useful in the clinic to detect tumors at small sizes, for lymph node assessment and for the detection of occult metastases.

Optical imaging techniques have been developed for laboratory studies but have recently been extended to humans. SPECT (Single Photon Emission Computed Tomography) is a well accepted clinical tool for which agents and methods exist for the characterization of disease in the clinical environment. The successful translation to the clinic depends upon further advances in crucial technical properties (imaging characteristics, sensitivity and specificity). We will specifically study how the dual modality images could be useful in tumor detection and treatment and develop techniques.

We report first our initial results in tomographic imaging of light emission. We present images showing that it is possible to detect small lesions not only subcutaneously but also at depth in vivo, and characterize the advantages of this method for quantitative imaging.

We have also demonstrated micro-SPECT (Single Photon Emission Computed Tomography) imaging at high resolution. We report here on our initial progress in SPECT, and on the advantages of tomography initially for small animals, showing submillimeter resolution in a mouse when imaging bone.

Dual Modality Imaging System

The gantry shown here supports both optical and SPECT imaging. The device rotates around its axis, the animal lies at the axis, and each camera records a view of the mouse. With four rotations we obtain twenty views, sufficient for a 3D image of the whole body. In this fashion we can visualize both the primary and metastases, when they develop.

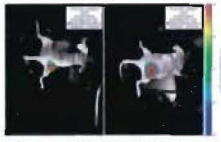

Images taken at different angles show substantially different light emission levels (2.4 vs $4.8\ 10^{10}$ RLU) indicating the usefulness of a tomographic architecture for the imager.

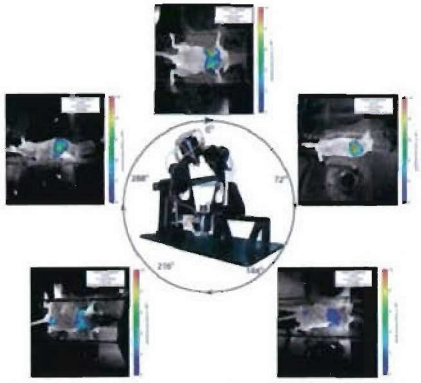

Five planar images obtained from specified angles showing bioluminescent signal overlaid on photographs of illuminated mouse. The nude mouse was implanted with A549-LUC human tumor cells. In total 20 images were acquired for 3-D reconstruction.

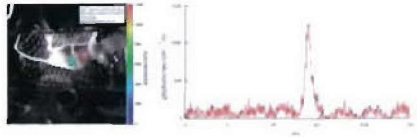

The cameras have high sensitivity, as shown in this BLI image of 5,000 MIA-Luc cells obtained in 8 minutes after administration of 450 mg/kg of Luciferin. The cells were injected in the pancreas of a BALBc mouse and occupy a volume some 6 mm in diameter. Note the high S/N.

Vascular Targeting Agent Experiments

Human breast cancer cells (MDA-MB-231-LUC) were implanted in the flank of a nude mouse. After the tumor was established it was imaged in 3D as the base line by administration of 450 mg/kg of Luciferin. The vascular targeting agent Combretastatin A 4-phosphate at 120 mg/kg i.p. was injected and the tumor imaged after 2 and respectively 24 hours.

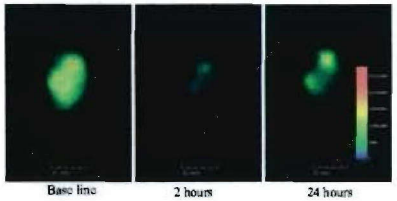

Base line 2 hours 24 hours

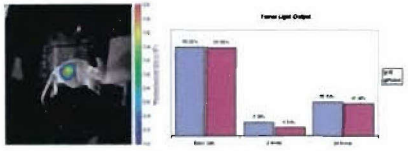

3D and planar imaging light output was used as a predictor of tumor activity and thus the efficiency of the vascular targeting drug.

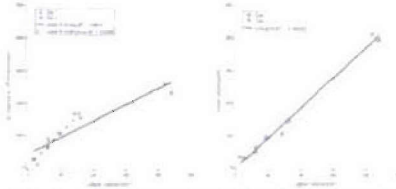

2D light intensity is a size-dependent predictor of tumor size even for a superficial tumors. The volume of the 3D reconstructed tumor is a much better linear predictor.

μSPECT Design

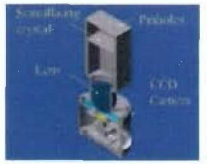

μSPECT camera includes multiple pinholes, CsI(Tl) scintillating crystal, optically coupled with the high sensitivity CCD camera.

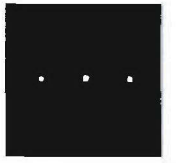

Pinhole planar image of two crossing 1-mm wide line sources filled with 400 uCi (14.8 MBq) ^{99}Tc each. Image obtained with 9 convergent pinholes (1.5 mm). Acquisition time 30 min.

Intrinsic Resolution

100 μm I-125 line source displaced 0.5 mm across crystal face. Profile through 0.375mm separation, x-axis in 0.15 mm pixels, y-axis in arbitrary digital units

Preliminary Results

Conclusions

We have reported our initial results in tomographic imaging of light emission. We have presented images showing that it is possible to detect small lesions not only subcutaneously but also at depth in vivo, and characterized the advantages of this method for quantitative imaging.

We have also demonstrated micro-SPECT (Single Photon Emission Computed Tomography) imaging at high resolution. We have reported here on our initial progress in SPECT, and on the advantages of tomography for small animals.

In the next two years we will develop these techniques further for in vivo imaging in the clinical setting.

Three Dimensional Light Emission Tomography (LET) using Multiple Rotating CCD Cameras

Edmond Richer, Nikolai Slavine, Matthew A. Lewis, Edward Tsyganov, Ginelle C. Gellert*, Z. Gunnur Dikmen*, Vikash Bhagwandin*, Jerry W. Shay*, Ralph P. Mason, Peter P. Antich

Departments of Radiology and *Cell Biology,
The University of Texas Southwestern Medical Center at Dallas, Dallas, TX

Introduction

Bioluminescent imaging of luciferase-expressing cells in living animals is a powerful technique for investigating molecular events, gene expression in living animals, cardiovascular development, assessing diverse promoter elements, and tumor growth and metastasis, etc [1, 2]. Current commercial instruments support planar imaging [3], but detection and study of the metastatic development at the earliest stages of disease, in small animal models, and the response to therapy demand higher sensitivity and resolution in the context of noninvasive whole-body imaging.

A three-dimensional imaging approach would greatly enhance applications in biomedicine since light-emitting cell populations would be better associated with specific organs and tissues and because depth-dependent corrections for quantitative light output can be included in the technique.

LET Imaging Device

A significant problem in detecting the light emitted from a tumor or organ inside an animal is that intervening tissues can totally or partially obscure light emitted in the direction of imaging [4]. Moreover, investigations using planar imaging show considerable variability between successive tests and animals [5]. The light may, however, be recovered from other viewing angles and thus, it is important to observe the animal from as many directions as possible. We therefore designed an optical imaging system with multiple high sensitivity CCD cameras that surround the subject in the transverse plane permitting the simultaneous acquisition of images from multiple angles. A computerized system can rotate the cameras around the longitudinal axis to provide a more complete angular coverage (Fig. 1). The images obtained at each angle are calibrated in units of total radiance, photons/sec/cm²/sr. For the 3D reconstruction, we connect pixel centers to the focal point of the objective used and backproject the lines into the object volume. 3D images are reconstructed using a Maximum Likelihood Expectation Maximization (ML-EM) method followed by scattering corrections using a deconvolution approach. The 3D image provides the bioluminescence flux in photons/sec, and using the average bioluminescent signal for a single cell one can estimate the total number of light emitting cells.

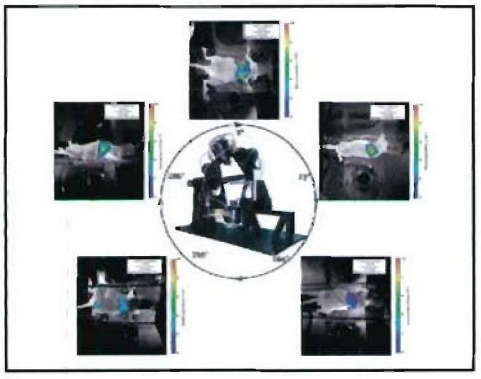

Figure 1.
Five planar images obtained from specified angles showing bioluminescent signal overlaid on photographs of illuminated mouse. The nude mouse was implanted with A549-LUC human tumor cells as a lung metastasis model.

In Vivo Experimental Results

A549-LUC human lung tumor cells (10^6) were injected IV in a nude mouse (BALB/cnu/nu). After 63 days the "lung metastases" were imaged following D-luciferin injection (450 mg/kg, SQ) in the anesthetized mouse. A set of 20 images, 18° apart, was obtained using 1 min exposure starting 3 min post-injection of D-luciferin. For each position an image of the mouse was obtained for co-registration, under external illumination.

Data reconstruction provides a 3-D model of the lung tumors (Fig 2). The algorithm was also applied to images obtained using light reflected from the skin under external illumination and the two data sets combined. Coronal cross-sections are presented in Figure 3, emphasizing the tomographic nature of the data and the wealth of information contained therein. Intense local foci are apparent with a more diffuse background distribution outlining the tumor-invaded areas of the lungs. Pathologic studies after sacrifice confirmed that A549-LUC tumor cells distributed throughout the various lobes of the lungs with multiple foci (Fig 4). A similar protocol was used to obtain a 3D reconstruction of Mia-LUC tumor cells implanted orthotopically in the pancreas, imaged after 18 days. In this case less luciferin was used (150 mg/kg, SQ injection) and the exposure time was 30 s per image.

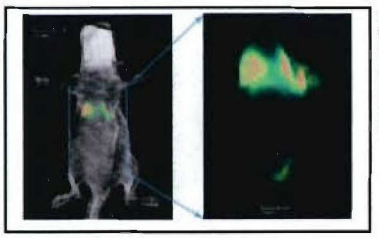

Figure 2.
Reconstructed BLI (right) and overlay on external light image (left). The anesthesia mask is seen covering the snout of the mouse (note the difference in scale).

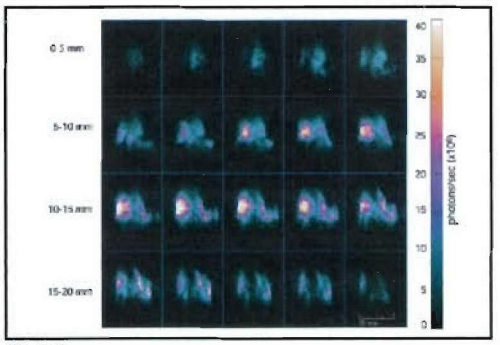

Figure 3.
Coronal cross-sections of bioluminescent data showing A549-LUC tumors in mouse lungs. The sections are 0.5 mm thick, 1 mm apart, and start dorsally (top left corner) ending ventrally (bottom right).

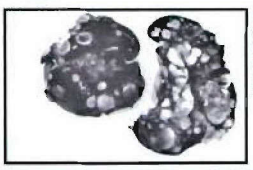

Figure 4.
Staining of intact lungs by injection of India ink directly into the trachea as well as serial sectioning of histological specimens indicates approximately 10^2-10^3 metastatic foci per mouse)

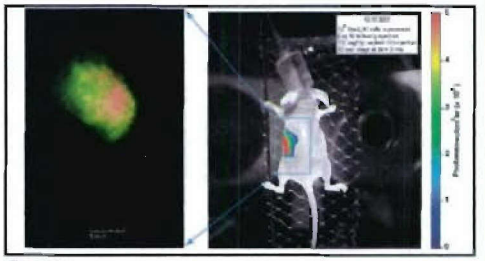

Figure 5.
Right: Bioluminescent pancreatic tumor image superimposed on image of the animal. This represents only one of 20 acquired images.
Left: 3D reconstruction of the light-emitting tumor (note the difference in scale).

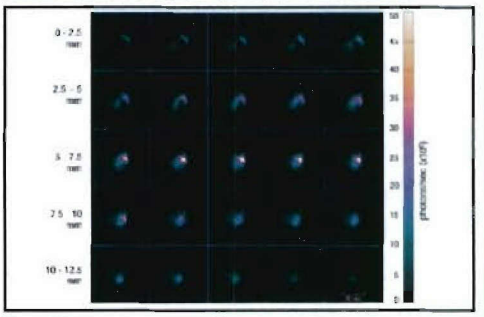

Figure 6.
Coronal cross-sections of pancreatic tumor in mouse. The sections are 0.5 mm thick, 0.5 mm apart, and start dorsally (top left corner) ending ventrally (bottom right).

Conclusions

We have demonstrated the feasibility of visualizing luciferase expressing cells at depth in a living mouse in 3-D. The three-dimensional and tomographic images provide better quantification of the light emission than traditional planar imaging techniques. This enhances the ability to assess and monitor spatio-temporal characteristics of tumor growth, identifying metastases, and potentially determining the effectiveness of cancer treatment. Beyond cancer, this methodology can be used to follow the fate of cells implanted at depth, such as stem cells.

The technique is capable of further increasing the usefulness of bioluminescence imaging, a modality which applies to a multitude of biological processes (e.g., bacteria, tumor cells, immune cells, genes, etc.) tagged with a reporter gene that encodes one of a number of light-generating enzymes (luciferases).

Acknowledgments

We are grateful to Trung Nguyen, Billy Smith, Allen Harper, Serguei Seliounine, Xiufeng Li, Todd Seesbe and Dr. A. Zinchenko for assistance with technical development. This work was supported in part by funds from the Simmons Cancer Center and the Cancer Imaging Program P20 (Pre-ICMIC) CA 86354.

References

1. Contag, C.H. and B.D. Ross, It's not just about anatomy: in vivo bioluminescence imaging as an eyepiece into biology. J Magn Reson Imaging, 2002. 16(4): p. 378-87.
2. Hillal, N.E., N. Rubio, M. Martinez-Villacampa, and J. Blanco, Combined noninvasive imaging and luminometric quantification of luciferase-labeled human prostate tumors and metastases. Lab Invest, 2002. 82(11): p. 1563-71.
3. Troy, T., D. Jekic-McMullen, L. Sambucetti, and B. Rice, Quantitative comparison of the sensitivity of detection of fluorescent and bioluminescent reporters in animal models. Molecular Imaging, 2004. 3(1): p. 9-23.
4. Massoud, T.F. and S.S. Gambhir, Molecular imaging in living subjects: seeing fundamental biological processes in a new light. Genes Dev, 2003. 17(5): p. 545-80.
5. Paroo, Z., R.A. Bollinger, D.A. Brasech, E. Richer, D.R. Corey, P.P. Antich, and R.P. Mason, Validating Bioluminescence Imaging as a High-Throughput, Quantitative Modality for Assessing Tumor Burden. Molecular Imaging, 2004. 3(3): p. 117-124.

Please visit other posters from this group at: #199, 200, 207, 216.

For further information, you may contact Edmond Richer at: edmond.richer@utsouthwestern.edu

Chapter 13

COMPARISON OF CsI(Tl) AND SCINTILLATING PLASTIC IN A MULTI-PINHOLE/CCD-BASED GAMMA CAMERA FOR SMALL ANIMAL LOW ENERGY SPECT

Edmond Richer, Matthew A. Lewis, Billy Smith, Xiufeng Li, Serguei Seliounine, Ralph P. Mason and Peter P. Antich
*University of Texas Southwestern Medical Center at Dallas**

1. INTRODUCTION

SPECT with submillimeter resolution (μSPECT) is needed for small animal imaging and differs from clinical SPECT - a rich and well established methodology of nuclear medicine - in that its focus is on the specific requirements of high resolution imaging over small distances with matching sensitivity, requiring differences in collimator schemes and image reconstruction methods specialized for that task. Current efforts towards this goal have focused on adapting established technologies from clinical to animal imaging. Currently available devices have resolution in the range of 1-3 mm and adequate sensitivity, but we believe that these parameters should be improved to facilitate molecular imaging. Prototypes are being developed [Ogawa et al., 1997; Ogawa et al., 1998; MacDonald et al., 2001; McElroy et al., 2001; Schramm et al., 2001] in response to a rising level of interest by pharmaceutical companies and molecular biologists (Russo, 1998).

Nevertheless, a significant factor for penetration of μSPECT into general usage remains the cost and ease of use of a system with adequate resolution for studies in mice and rats. In the case of small animal imag-

*Partial funding provided by NCI P20 CA 86354

ing, pinhole collimator and a closed detector-object configuration can be used with SPECT. This presents the advantage to minimize the time for data collection, allowing a superior detector sensitivity at high spatial resolution by using multiple pinholes and crystals. A pinhole size of 0.5 mm would provide the sub-millimeter resolution required to study small animals such as mice.

2. CCD-BASED GAMMA CAMERA

With the goal of achieving high resolution with appropriate sensitivity for use in small animal studies, we have developed a multi-pinhole gamma camera based on thallium-doped cesium iodide [CsI(Tl)] crystals and wavelength-matched charge-coupled devices (CCDs).

A Scientific Imaging Technologies Inc. (SITe) SIA502AB1 CCD, a 512x512 pixels, non-color, back-illuminated, full frame image sensor was selected due to its excellent sensitivity (greater than 85 % quantum efficiency from 400 nm to 750 nm). The pixel size is 24 x 24 μm providing a large well capacity of 350,000 e^-. Coupled with a good sensitivity (2.6 $\mu V/e^-$), low dark current (20 pA/cm^2 at 20°C), and low readout noise (5 e^-) this provides a dynamic range of 70,000, more than full 16 bits.

The CCD is be incorporated into a self-contained, cooled camera, equipped with electronic circuitry and optics. The principal method for noise suppression with CCD technology is cooling the chip itself. In our proposed implementation, the CCD camera employs a five stage thermoelectric cooling element equipped with a controller circuit that keeps the operational temperature of the CCD at -40°C. An external heat exchange unit eliminates the generated heat. The net effect will be a substantial reduction of the dark noise generated inside the CCD, and thus better image quality and longer possible exposures. The internal chamber of the camera is kept under vacuum to allow better cooling and eliminate ice crystals formation on the sensitive element.

The light exposure is controlled using a mechanical shutter. The shutter allows for short exposure times, down to 5 msec, which are not attainable when an electronic shutter is employed. Also, the mechanical shutter prevents light from affecting the CCD during the readout phase, thus eliminating the smear effect observed in full frame CCD cameras without a shutter. To widen the dynamic range, the CCD readout employs a 16-bit A/D conversion chip equipped with a low noise preamplifier and correlated double sampling circuitry. This architecture provides high dynamic range combined with very low readout noise. Finally, a flexible pixel binning scheme is implemented allowing for better signal to noise ratio in the extremely low light level conditions that expected

with higher resolution imaging. Optical coupling of the CCD to the scintillating crystal is implemented using an off-the-shelf low reflectance optical lens.

We selected CsI(Tl) as the scintillator rather than the more traditional gamma camera scintillator, NaI(Tl). NaI(Tl) has a scintillation wavelength of maximum emission at 415 nm, ideally matched to the efficiency profile of photomultiplier tubes (PMTs), which have a typical quantum efficiencies of 20%. CsI(Tl), on the other hand, has a maximum emission at 550 nm, which is well into the region where solid-state detectors are dominant. While most scintillator property tables list CsI(Tl) as having 45% the photoelectron yield as compared to NaI(Tl), this comparison is deceptive as it holds true only for PMTs; using CCDs, the light yield of CsI is 53% higher than NaI. Further advantages are sturdier mechanical properties, limited hygroscopicity, and higher density. This last factor will allow thinner scintillators with the same capture efficiency.

Two potential drawbacks exist for this gamma camera design, intrinsic to the scintillator and the detector. First, CsI(Tl) is a slow scintillator (900 ns versus 230 ns for NaI(Tl)). However, this is not a problem since timing and triggering is not needed because the CCD is an integrating device, and subsequently an exposure will contain the recorded detection of many high energy photons. Second, and more importantly, energy discrimination is not possible. Two facts make its application to mouse imaging possible and free of excessive scatter contributions. First, our major applications of the proposed μSPECT is to I-125 imaging, in which case the existence of a K-edge at 32.2 keV for the crystal is sufficient to accept the 35 keV gamma emitted by this nuclide and reject lower energy noise. Second, the completed system is not intended for use in humans, where gamma rays have an appreciable probability of scatter before exiting the body, but for a small animal, so that scatter rejection is less important and can be accounted for with absorption corrections.

The intrinsic resolution of the gamma detector was determined using a 100 μm slit collimator displaced across the surface of the scintillating crystal using a micrometric positioning device. Figure (13.1) shows the image from a I-125 line source displaced 0.5 mm across crystal face. The corresponding profile is presented in Fig. (13.2). The intrinsic resolution of the camera was determined to be below 0.4 mm (see Antich et al., 2003). Considering a field a view of 50 mm, suitable for an animal the size of a mouse, the number of pixels required to record an image in a non magnifying geometry is less than 128. Comparing with the much higher resolution of the CCD (512x512 pixels) one concludes that a set of up to 16 pinhole projections can be acquired on a single CCD image.

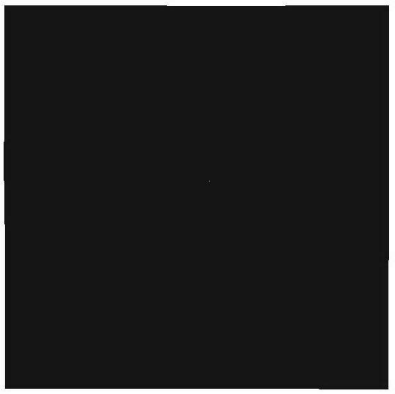

Figure 13.1. 100 μm I-125 line source displaced 0.5 mm across crystal face.

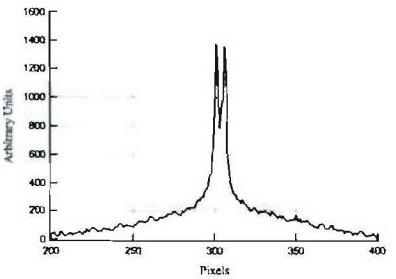

Figure 13.2. Profile of the line source displaced 0.5 mm across crystal face.

Thus, in our design, collimation is provided by a 3x3 array of pinholes that provide some field-of-view overlap in the transverse plane, but are non-degenerate in the longitudinal axis of the animal. A schematic rendering of the geometry of this set-up and an actual multiple-pinhole image is shown in Figs.(13.3) and (13.4).

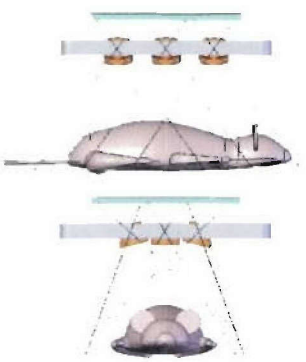

Figure 13.3. Field of view of pinhole collimators.

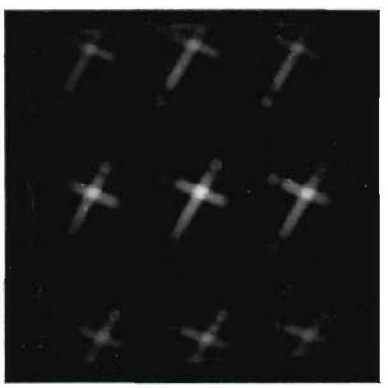

Figure 13.4. Convergent 9-pinhole (1.5 mm) collimator, 2 400 μCi (14.8 MBq) line sources, 30 minute acquisition.

3. PLASTIC SCINTILLATORS

For imaging with low energy iodine-125 labeled agents (<35.5 keV), we further consider scintillating plastic as an alternative to CsI(Tl). Plastic scintillators have the advantage of being mechanically sturdier than crystals, have less hygroscopicity, and more importantly can be shaped in any desired shape and dimension. Moreover, the light emission can be tuned to the optimum wavelength sensitivity of the CCDs using waveshifting doping materials. A potential drawback is their lower density, which require thicker scintillators to achieve a good detector cross-section with negative effects on resolution.

In order to determine the efficiency of the plastic scintillators we compared the light output produced by a 125-I line source (400 μCi) in direct contact with a 5.6 mm BC-408 scintillator (Bicron Inc.) and a 2 mm CiI(Tl) crystal. The light output normalized to the thickness shows a factor of 237 in favor of the CsI(Tl) crystal.

A set of PVT based scintillators containing different microcrystals in two concentrations were also tested with the results presented in Table (13.1). The concentration is given in mg of microcrystal material per g of PVT, and the light output in arbitrary light units per minute of exposure (ALU/min) as obtained from the CCD camera. The light output normalized to the scintillator material thickness is also presented. All tested microcrystals significantly improved the efficiency of the scintillator, with LSO in 100 mg/g concentration showing spectacular results, increasing the thickness normalized light output almost 600 times compared to the PVT alone. Comparing the PVT containing LSO with the CsI(Tl) crystal we observed that while the total light output is larger for the crystal by a factor of 2.26 the normalized light output is higher for the PVT containing LSO by a factor of 1.58.

Table 13.1. Comparison of plastic scintillators light output with different microcrystals.

Microcrystal Material	*Microcrystal Concentration*	*Thickness [mm]*	*Light Output [ALU/min]*	*Normalized Light Output*
ErSO	50	0.5	375	750
ErSO	100	0.5	625	1,250
YbSO	50	0.35	525	1,500
YbSO	100	0.35	888	2,537
LSO	50	0.35	10,125	28,929
LSO	100	0.35	16,065	45,900
None	0	5.6	431	77

The intrinsic resolution of the scintillating plastic LSO/CCD-coupled gamma camera was determined by the same method to be <0.5 mm, comparable to our previously reported results for the CsI(Tl) based detector. An image of 2 400 μCi (14.8 MBq) line sources, obtained using LSO 100 mg/g scintillator and a 1.5 mm pinhole collimator is presented in Fig. (13.5).

Figure 13.5. Pinhole (1.5 mm) collimator, 2 400 μCi (14.8 MBq) line sources, 30 minute acquisition.

A potential problem with the natural radioactive background of ^{176}Lu in LSO has been identified with single photon imaging [Huber et al., 2002]. However, since the natural background radiation spectrum is primarily above 300 keV, the thin section of the doped plastic scintillator will minimize unwanted noise from this source.

4. CONCLUSIONS AND FUTURE WORK

We have made considerable progress in designing and constructing devices which will allow us to compare quantitatively different designs and technologies for high resolution, high sensitivity μSPECT. In future studies we will optimize with respect to the resolution and sensitivity the plastic scintillator thickness and the microcrystal concentration.

Challenges also remain in the development of the image reconstruction algorithms suitable for multiple-pinhole CCD-based μSPECT cameras.

References

Antich, P. P., Lewis, M. A., Richer, E., Kulkarni, P. V., Smith, B., and Mason, R. P. (2003). A novel multi-pinhole/CCD-coupled CsI(Tl) crystal gamma camera for fully 3D μSPECT / μCT small-animal imaging. In *Proceedings of the 50th Annual Meeting of Society of Nuclear Medicine.*

Huber, J. S., Moses, W. W., Jones, W. F., and Watson, C. C. (2002). Effect of ^{176}Lu background on singles transmission for LSO-based PET cameras. *Phys. Med. Biol.*, 47:1–7.

MacDonald, L. R., Patt, B. E., Iwanczyk, J. S., Tsui, B. M. W., Wang, Y., Frey, E. C., Wessell, D. E., Acton, P. D., and Kung, H. F. (2001). Pinhole SPECT of mice using the LumaGEM gamma camera. *IEEE Transactions on Nuclear Science*, 48(3):830–836.

McElroy, D. P., MacDonald, L. R., Beekman, F. J., Wang, Y., Patt, B. E., Iwanczyk, J. S., Tsui, B. M. W., and Hoffman, E. J. (2001). Evaluation of A-SPECT: A desktop pinhole SPECT system for small animal imaging. In *IEEE Nuclear Science Symposium Conference Record*, volume 3, pages 1835–1839.

Ogawa, K., Kawade, T., Nakamura, K., Kubo, A., and Ichihara, T. (1997). Ultra high resolution pinhole SPECT. In *IEEE Nuclear Science Symposium and Medical Imaging Conference*, volume 2, pages 1600–1604.

Ogawa, K., Kawade, T., Nakamura, K., Kubo, A., and Ichihara, T. (1998). Ultra high resolution pinhole SPECT for small animal study. *IEEE Transactions on Nuclear Science*, 45(6):3122–3126.

Russo, E. (1998). Going micro: Imaging devices to benefit both mouse and biologist. *The Scientist*, 12(21):1.

Schramm, N., Wirrwar, A., and Halling, H. (2001). Development of a multi-pinhole detector for high-sensitivity SPECT imaging. In *IEEE Nuclear Science Symposium*, volume 3, pages 1585–1586.

Chapter 26

Projection and Pinhole based Data Acquisition for Small Animal SPECT using Storage Phosphor Technology

M A Lewis, G Arbique, E Richer, N Slavine, M Jennewein*, A Constantinescu, R Brekken, J Guild, E N Tsyganov, R P Mason, and P P Antich

The University of Texas Southwestern Medical Center at Dallas

1. Introduction

Three-dimensional Single Photon Emission Computed Tomography (SPECT) can provide high-resolution insight into biomolecular distribution and pharmacokinetics. However, instrument availability and distribution is limited at present, and imaging times can be considerable. To evaluate the large array of novel agents which are becoming available, we find that storage phosphor-based *in vivo* imaging can provide an important, rapid-throughput transition from the traditional *ex vivo* sacrifice/gamma-counting and autoradiography to full time-course SPECT.

Storage phosphor (SP) technology has found wide-spread usage in both the radiology clinic and in the molecular biology laboratory. With a linear sensitivity latitude exceeding that of plain film, photostimulable luminescence (PSL) screens can facilitate high-throughput screening and autoradiography for a variety of small animal models. Despite the impressive growth and improvement in small animal nuclear imaging, the determination of appropriate time and duration of imaging for a given animal model and imaging agent is still crucial in study design and analysis. Storage phosphor technology is well-suited for addressing this issue, either by producing quantitative planar projection or low-resolution tomographic images. With γ-ray stopping cross-sections that

*primary affiliation: Johannes Gutenberg-Universität Mainz, Germany

are not radically different from film/screen systems, the phosphor image plate[1] is well-suited for low energy gamma detection, especially for imaging studies with iodine-125 (^{125}I) where tissue scattering is minimized.

2. Background

2.1 Storage phosphor technology

Photostimulable storage phosphor (PSP[2]) screens were developed and introduced in the 1980s [Sonoda et al., 1983] as a replacement for film/screen x-ray detection systems. Today, SP technology is the key component in commercial film-less imaging systems grouped under the generic term Computed Radiography (CR) [Arbique et al., 2003]. This technology is distinct from so-called Digital Radiography, where x-ray detection is digital from the moment of detection. Subsequently, SP technology was adopted by most suppliers of autoradiography equipment [Johnston et al., 1990]. While the average molecular biologist today does not have ready access to a small animal SPECT system, he or she most likely possesses or has available an SP scanner or reader that is routinely used for gel and blot applications. Compared to the standard CR reader in a radiology clinic, these scanners typically have higher spatial resolutions (down to 50 μm) and greater digital resolution (16 vs. 12 bit). Although the current trend is towards more expensive scanners that can also read direct- or chemi-fluorescence assays, a multipurpose SP system can be obtained for a fraction of the cost of a minimal small animal SPECT system.

A full physical description of SP technology, including image performance parameters (MTF, NPS,DQE) can be found elsewhere [von Seggern, 1999; Rowlands, 2002]. In summary, the interaction of a high-energy photon with a BaF(Br,I):Eu^{2+} phosphor grain generates electrons and holes that are trapped in the immediate fluorohalide matrix area. A latent image is formed in proportion to the density of the trapped carriers. Upon subsequent photostimulation using a red light source (typically a laser at 590-680 nm), the electron is liberated from its trap and recombines with a hole. The energy generated in this process is resonantly transfered to a doped Europium ion, which then decays with characteristic luminescence (390 nm). This luminescence is captured using a photomultiplier tube and digitized. With an appropriate reader, a typical SP image plate will have a linear dynamic range up to a thousand times greater than film, spanning 4-5 orders of magnitude, and reusable for tens of thousands of exposures. Due to thermal stimulation, the latent image does fade (decay constant approximately 9 hours), so immediate reading of PSL screens is advisable.

2.2 Low energy-integrating SPECT

The hypothesis of low energy-integrating SPECT is that reasonable images can be obtained using γ-ray detectors that integrate activity counts and have no energy discrimination for scatter rejection. Monte Carlo simulations [Tenney, 2002] have shown that for ^{125}I in a mouse-sized cylinder of water the scatter fraction remains below 40% and the detective quantum efficiency (DQE) is in the reasonable range of $0.6 - 0.7$, which can exceed the DQE of the SP screen [Rowlands, 2002]. Although dual isotope imaging is precluded, energy-integration imaging shifts the burden of work to image reconstruction, where scatter correction represents a significant challenge, but is an active area of research for all nuclear medicine modalities.

A CCD-based gamma camera has been recently proposed as an efficient energy-integrating detector for small animal SPECT. Although a CCD-based camera will in general be less expensive than the traditional position-sensitive PMT, the intrinsic resolution of the CCD design will be significantly better, with characteristic resolutions below 400 μm [Antich et al., 2003]. At these low intrinsic resolutions, parallel-hole collimators are not well-matched. In addition, compared to a non-magnifying pinhole geometry, the packing of multiple, static projection is limited.

For lower resolution, high-throughput screening, we find that SP image plates and screens are an acceptable alternative to CCDs in an energy-integrating detector. If an infrastructure for reading SP technology is already in place, then the relative cost for detectors is further reduced, with no sacrifice in intrinsic resolution. With this savings, we believe that small animal SPECT using SP technology may be possible for routine low-resolution, high-throughput screening.

3. Prototype

Recently, a prototype system using CR image plates for co-registered I-125 planar scintigraphy and x-ray radiography was introduced [Boone et al., 2003]. In this scheme, half of the image plate is used for a planar emission image. After exposure, the image plate is precisely translated so that a transmission radiography can be taken with the other half of the plate. These two images are subsequently co-registered in software, using the known displacement.

Our approach differs in that we have utilized custom-sized SP image plates as energy-integrating detectors in a low-resolution small-animal pinhole emission computed tomography geometry. As shown in Figure 26.1, a 30 mm inner diameter/5 mm thick brass cylinder serves as a support for eight 1.5 mm diameter pinholes (also in brass, with 90°

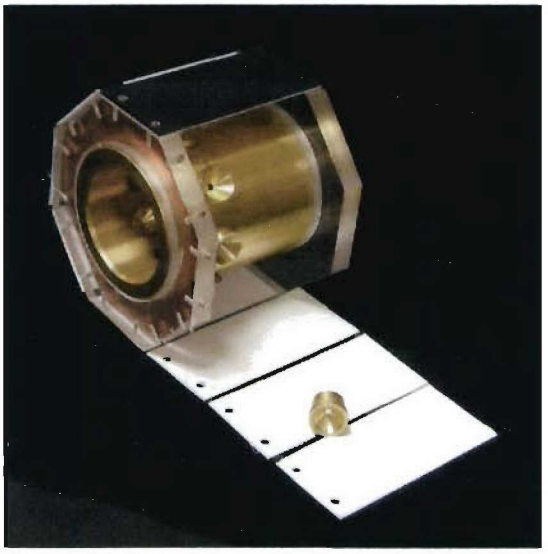

Figure 26.1. Prototype murine pinhole emission computed tomography system using using energy-integrating storage phosphor technology

cone of acceptance), spaced in 45° increments around a ring. In this geometry, the field-of-view in a plane intersecting the axis of the cylinder is equivalent to the 30 mm diameter of the cylinder. A strip of 8 small SP image plates is attached to the support structure at fixed points of known distance from the pinhole centers. Each detector is placed 10 mm from the corresponding pinhole center. In this geometry, reading of the SP screen at 100 μm resolution will produce 128x128 and 256x128 projections for 60° and 90° cone-of-acceptance pinholes, respectively. For ^{125}I energies ($<$ 35.5 keV), brass is sufficient for collimation (HVL $\approx 80\mu$m).

Eight 24 mm by 50 mm SP screens were cut from a 25.2x30.3 cm Fuji CR ST-VN Imaging Plate (Fuji Photo Film, Tokyo). Attachment holes of 1.6 mm diameter were milled at the end of each screen for attachment to the imaging system. The imaging plates were connected in a continuous strip using black insulating tape.

The system is placed in a light-tight enclosure with the phantom or animal placed inside the cylinder. After exposure[3], the SP detector is carefully removed and transported in a light-tight envelope to the SP reader. A SP scanner with the ability to read arbitrary size screens, such at the Molecular Dynamics Storm (Amersham Biosciences, Piscataway, NJ), is preferred, but in practice other systems may work. Special

Figure 26.2. Eight pinhole projections from two 1.85 MBq ^{125}I capillaries (0.8 mm inner diameter). 15 minutes integration exposure. Signal-to-noise ratio ≈ 10
. Heterogeneities due to air bubbles in capillaries and infiltration of sealant.

attention to the relationship between the detector coordinate system and the angular position of the detector should be maintained, as different SP readers may report data in mirror orientations.

4. Results

To evaluate the prototype system, two non-uniform 1.85 MBq ^{125}I capillaries with inner diameter of 0.8 mm were prepared. The line sources were placed off-center in the field-of-view for the ring of pinholes, and were non-parallel with an average separation of 8 mm. The sources were imaged for 15 minutes, followed by prompt reading of the SP image plates. Eight pinhole projections of the line source can be found in Figure 26.2.

Using unexposed regions of the SP image plates, background noise levels were determined for windowing. Since the attachment holes appear as voids on the raw projection images, detector coordinate origins were calculated as the midpoint, and projections were corrected for rotation. A 3D image (48x48x60, 0.5 mm voxels) was reconstructed from these eight projections using the maximum-likelihood estimation maximization (MLEM) algorithm with convolution for resolution modelling [Reader et al., 2002; Zinchenko et al., 2003]. Figure 26.3 provides a maximum intensity projection (MIP) of the reconstructed volume that is consistent with the projections in Figure 26.2. For a non-magnifying pinhole geometry, the standard pinhole collimator resolution expression

$$R_c = \frac{a+b}{a} d_e \tag{26.1}$$

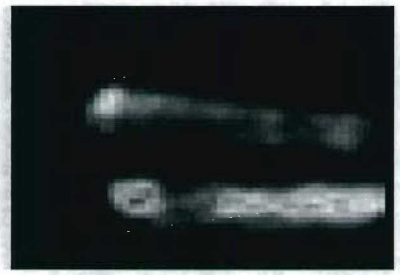

Figure 26.3. Maximum intensity projection for reconstructed, heterogenous line sources

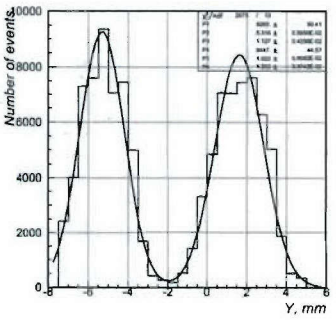

Figure 26.4. Cross section through line sources with expected broadening due to pinhole geometry

(a is the pinhole to detector distance, b is the pinhole to object distance) indicates that the pinhole point-spread function (full-width half-maximum) at the imaging volume center is 2.5 times the pinhole diameter. Figure 26.4 demonstrates the observed and expected line broadening due to the non-magnifying geometry.

5. Conclusions and Open Issues

Low resolution imaging with a static pinhole geometry and energy-integrating storage phosphor detectors is a feasible, low cost alternative for high-throughput evaluation of imaging agents and for determining optimal timing of high resolution, small animal SPECT studies. High resolution is not limited by the intrinsic resolution or sensitivity of the SP detector, but is due to limited angular sampling with small numbers of projections.

The current prototype possesses detector areas that allow for expansion to 2 rings of 90° or 3 rings of 60° pinholes. The challenge for higher resolution is to increase angular sampling by increasing the number of projections in the static geometry. Sixty projections has been reported as sufficient for imaging [Palmer and Wollmer, 1990], but multiplexed multi-pinholes [Schramm et al., 2001], coded-apertures [Schellingerhout et al., 2002], and relaxed collimation [Prior et al., 1993] are possible solutions for efficient projection packing.

For low exposures with PS image plates, it has been shown that noise levels obey the expected Poisson statistics [Arbique et al., 2003].

However, at uniform higher exposures, it has been demonstrated that structured noise source in the image plate contributes to spatial-variant signal-to-noise ratio [Nishikawa and Yaffe, 1990]. A procedure for correcting projection images in the pre-processing stage has not been addressed.

BaF(Br,I):Eu^{2+} SP imaging plates are optimized for 80 kVp radiography. Unfortunately, a large K-edge at 40 keV reduces the sensitivity of SP detectors to ^{125}I emissions. The future commercial availability of storage phosphors more suitably matched to low energy emissions (RbCs:Tl^{+} and CsBr:Eu^{2+}) will increase the efficiency of energy-integrated imaging with ^{125}I.

As stated above, the primary challenge remains development of image reconstruction algorithms that provide scatter correction. Inevitably, this will probably require knowledge of the mouse topography (size and shape) for modelling scatter on a per-animal basis.

Acknowledgments

This work was supported in part by NCI P20 CA 86354.

Notes

1. The terms *screen* and *image plate* are synonymous in the context of this paper

2. The terms *storage phosphor* (SP), *photostimulable luminescence* (PSL), and *photostimulable storage phosphor* (PSP) are synonymous in the context of this paper.

3. Exposure time will depend upon collimation. Our experience is that 1 minute per 2 μCi is typically sufficient

References

Antich, P. P., Lewis, M. A., Richer, E., Kulkarni, P. V., Smith, B. J., and Mason, R. P. (2003). A novel multi-pinhole/CCD-coupled CsI(Tl) crystal gamma camera for fully 3D μSPECT/μCT small-animal imaging. *Journal of Nuclear Medicine*, 44(5 (Supplement)):161P. No. 523. Presented at 2003 SNM Annual Meeting, New Orleans, LA, June 21–25.

Arbique, G., Guild, J., Anderson, J., Blackburn, T., Lane, T., and Wang, J. (2003). Clinical experience with a FUJI computed radiography quality assurance program. *Medical Physics*, 30(6):1344. Presented at 2003 AAPM Annual Meeting, San Diego, California, August 10–14.

Boone, J. M., Abbey, C. K., and Cherry, S. R. (2003). A combined I-125 nuclear emission and transmission radiography system for co-registered imaging of mouse function and anatomy. *Medical Physics*,

30(6):1438–1439. Presented at 2003 AAPM Annual Meeting, San Diego, California, August 10–14.

Johnston, R. F., Pickett, S. C., and Barker, D. L. (1990). Autoradiography using storage phosphor technology. *Electrophoresis*, 11(5):355–360.

Nishikawa, R. M. and Yaffe, M. J. (1990). Effect of various noise sources on the detective quantum of phosphor screens. *Medical Physics*, 17(5):887–893.

Palmer, J. and Wollmer, P. (1990). Pinhole emission computed tomography: method and experimental evaluation. *Phys. Med. Biol.*, 35(3):339–350.

Prior, J. O., Antich, P. P., Fernando, J., Anderson, J. A., Kulkarni, P. V., and Parkey, R. W. (1993). Imaging stategies with scintillating fibers detectors: issues and preliminary results. In *Scintillating Fiber Technology and Applications. SPIE.*, volume 2007, pages 116–124.

Reader, A. J., Ally, S., Bakatselos, F., Manavaki, R., Walledge, R. J., Jeavons, A. P., Julyan, P. J., Zhao, S., Hastings, D. L., and Zweik, J. (2002). One-pass list-mode em algorithm for high resolution 3D pet image reconstruction into large arrays. *IEEE Trans. Nucl. Sci.*, 49:693–699.

Rowlands, J. A. (2002). The physics of computed radiography. *Phys. Med. Biol.*, 47(23):R123–R166.

Schellingerhout, D., Accorsi, R., Mahmood, U., Idoine, J., Lanza, R. C., and Weissleder, R. (2002). Coded aperture nuclear scintigraphy: A novel small animal imaging technique. *Molecular Imaging*, 1(4):344–352.

Schramm, N., Wirrwar, A., and Halling, H. (2001). Development of a multi-pinhole detector for high-sensitivity SPECT imaging. In *IEEE Nuclear Science Symposium*, volume 3, pages 1585–1586.

Sonoda, M., Takano, M., Miyahara, J., and Kato, H. (1983). Computed radiography utilizing scanning laser stimulated luminescence. *Radiology*, 148(3):833–888.

Tenney, C. R. (2002). On the use of an energy-integrating detector for small-animal pinhole emission computed tomography. Presented at 2002 Annual Conference of the Academy of Molecular Imaging, San Diego, CA, October 22–27.

von Seggern, H. (1999). Photostimulable x-ray storage phosphors: a review of present understanding. *Brazilian Journal of Physics*, 29(2):254–268.

Zinchenko, A., Tsyganov, E. N., Slavine, N. V., Kulkarni, P. V., Lewis, M. A., Mason, R. P., Oz, O. K., Parkey, R. W., and Antich, P. P. (2003). Expectation maximization algorithm with resolution decon-

volution for 3-D image reconstruction in a small animal PET imager. *Journal of Nuclear Medicine*, 44(5 (Supplement)):161P. No. 528. Presented at 2003 SNM Annual Meeting, New Orleans, LA, June 21–25.